


Research Article

Stress Analysis and Structural Optimization of Steel–Concrete Joint of Zhonghua Road Bridge in Liaocheng

Jie Jin,¹ Junlin Zhang,² Ye Li,² Zengkui Xie ,³ and Lipo Yang⁴

¹Institute of Architectural and Engineering of Liaocheng University, Liaocheng 252001, China

²Beijing Engineering CoMPany Limited of China Railway Urban Construction Group, Beijing 100024, China

³CCCC Highway Bridges National Engineering Research Centre Co., Ltd., Beijing 100088, China

⁴Tianjin Municipal Engineering Design & Research Institute, Tianjin 300392, China

Correspondence should be addressed to Zengkui Xie; xiezengkui123@gmail.com

Received 4 October 2022; Revised 25 June 2023; Accepted 26 June 2023; Published 28 July 2023

Academic Editor: Ying Qin

Copyright © 2023 Jie Jin et al. This is an open access article distributed under the Creative Commons Attribution License, which permits unrestricted use, distribution, and reproduction in any medium, provided the original work is properly cited.

Based on Zhonghua Road Bridge in Liaocheng city, a single tower hybrid cable-stayed bridge, the stress of the steel-concrete joint of the girder is studied using the finite element method with the software MIDAS and ANSYS. The beam element model of the whole bridge is established in MIDAS CIVIL, from which the internal forces of the critical sections of the steel–concrete joint under six adverse conditions are obtained. Then, the results are applied in the refined solid-shell finite element model established in ANSYS. With the stress analysis, it is found that when the steel–concrete joint is used in the girder of the single tower cable-stayed bridge, both the compressive strength of concrete and the tensile strength of steel can be fully used, and the structural stiffness can be smoothly transferred through the two different materials in the joint, which makes the structural behavior more reasonable. The detailed stress analysis also shows that it is prone to generate considerable stress concentration at the corners and the connection between the steel lattice chamber and the pressure bearing plate, and the concentration can be avoided by local stiffening and smoothing of the chamfers. The sensitivity analysis of the web thickness in the joints and bearing plates showed that increasing the thickness of the intermediate web would lead to a moderate reduction in the stress of the web itself, while the stress in the steel member remained relatively constant. However, when the thickness of the bearing plate is increased from 60 to 80 mm, the stress of each part of the steel plate in the steel grid will be significantly reduced, and the maximum reduction can reach 48%. The improvement of concrete strength has little effect on the stress of the steel cell, and the C50 concrete strength grade used in the design is more reasonable.

1. Introduction

Cable-stayed bridges are commonly used for large-span structures, and they exhibit distinct structural characteristics: beam bending, tower compression, and cable tension. Each component plays a specific mechanical role, enabling cable-stayed bridges to achieve extraordinary spanning capabilities. As a high-order statically indeterminate structural system, the span allocation of a cable-stayed bridge has a profound influence on the stress distribution of its main girder [1–3]. When adjacent spans have a significant difference in length, adopting a hybrid girder configuration for the main girder is a reasonable choice. In this case, the main girder with a larger span is typically a steel box girder, which is lightweight,

exhibits high flexural carrying capacity, and has large stiffness, while the side spans are usually constructed using prestressed concrete box girders, which are heavier but have moderate spanning capabilities [4, 5]. To achieve a reasonable transition in terms of materials and structural stiffness between the steel and concrete girders, a novel structural element called the “steel–concrete composite segment” has emerged. As a transitional structure designed with two different materials, the steel–concrete composite segment has a complex configuration and is located in a critical section of the entire bridge where both bending moments and axial forces are relatively high, making it an important segment affecting the overall bridge safety. Therefore, it is necessary to conduct in-depth research on the mechanical issues of the

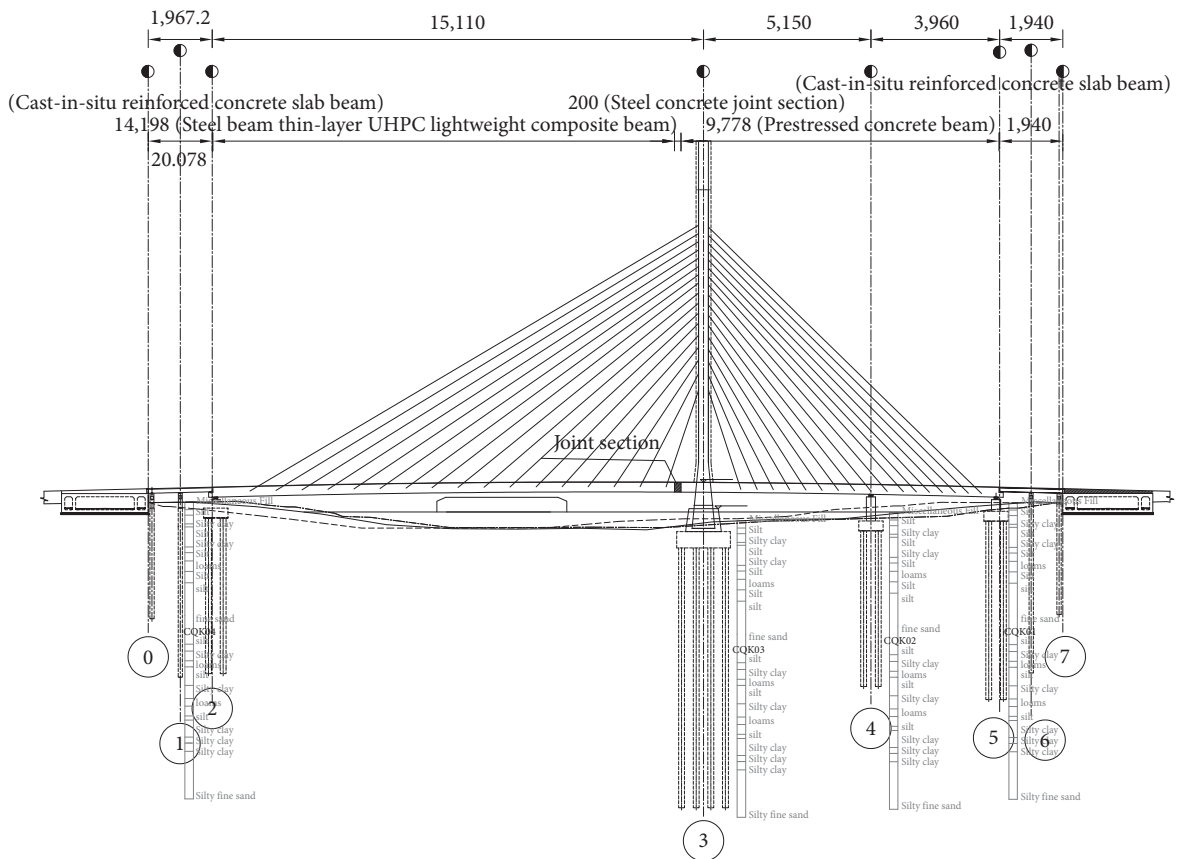


FIGURE 1: Elevation of Zhonghua Road Bridge in Liaocheng (unit: cm, the same below).

composite segment, such as load transfer mechanisms, stiffness characteristics, and stress distribution [6–8].

Currently, many scholars have studied the stress characteristics of steel–concrete composite segments [9–12]. However, there is limited research on the stress analysis of composite segments in large-span hybrid girder bridges composed of UHPC steel bridge decks and concrete girders. In this study, taking the Zhonghua Road Bridge in Liaocheng as an example, based on the overall calculation results obtained from MIDAS CIVIL, the corresponding internal forces are extracted. These internal forces are then applied to a refined finite element model of the steel–concrete composite segment, and appropriate constraints are defined for analysis and solution. The study aims to analyze the stress characteristics and load transfer mechanisms of the composite segment with a UHPC bridge deck system, providing references for the design of this type of bridge, and detailed analysis of the composite segment with a UHPC bridge deck system.

2. Project Overview

2.1. Elevation. Zhonghua road and Tuhai river have a skew angle of about 35° , with the inclined length of the river of about 280 m. The main bridge adopts a structure asymmetrical single-tower cable-stayed bridge with a full length of 244.4 m (including bracket), a span arrangement of $151.1 + 91.1$ m, and a ratio of side span to main span of 0.6. In order to

further reduce the mid-span moment of the side-span concrete box girder, an auxiliary pier is set 39.6 m before the side-span transitional pier. As there is a huge difference in span length between side and main spans, it is determined that hybrid girder is used as the main girder, while the main span is composed by the steel box girder and 5 cm-thick UHPC light composite girder, which is featured by light weight and large span. Moreover, its UHPC pavement thoroughly solves the problems of low stiffness and frequent cracking of traditional asphalt steel pavement; its side span adopts the prestressed concrete box girder scheme to effectively increase structural weight and side-span stiffness. A steel-UHPC steel–concrete joint is set up at a distance of 6.9 m away from the tower between main span and side span for the purpose of achieving a transition between these two kinds of structures.

The towers adopt steel structure; the left and right towers have a height of 105.12 and 120.12 m, respectively, with a difference of 15 m between them. A steel girder is set up below 90.12 m of the tower bottom to increase the transverse stability of the tower. The overall layout of Zhonghua Road Bridge is shown in Figures 1 and 2.

2.2. Cross-Section. The main span's steel box–UHPC thin and lightweight composite beam has a height of 3.05 m, while the side-span's concrete box girder is 3 m in height; both adopt single-box four-chamber section. The standard girder



FIGURE 2: Actual project photos of Zhonghua Road Bridge in Liaocheng.

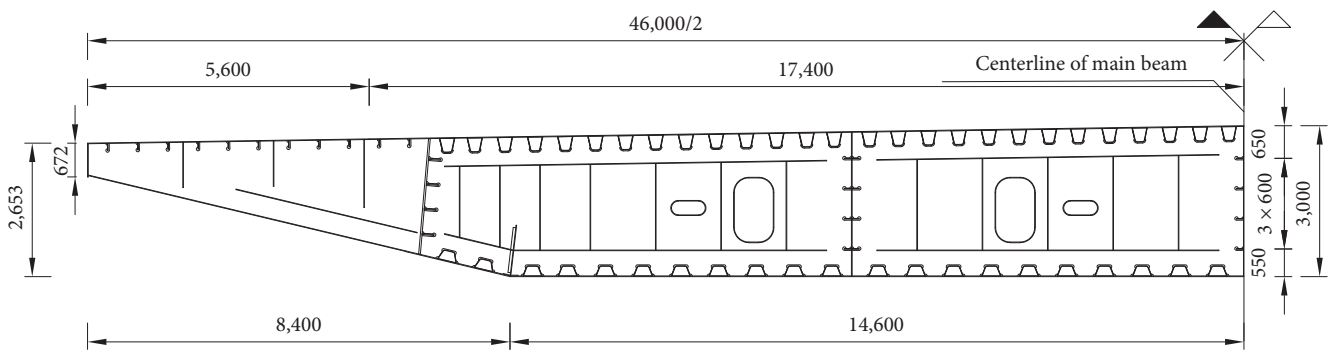


FIGURE 3: Standard cross-section of main span steel box girder.

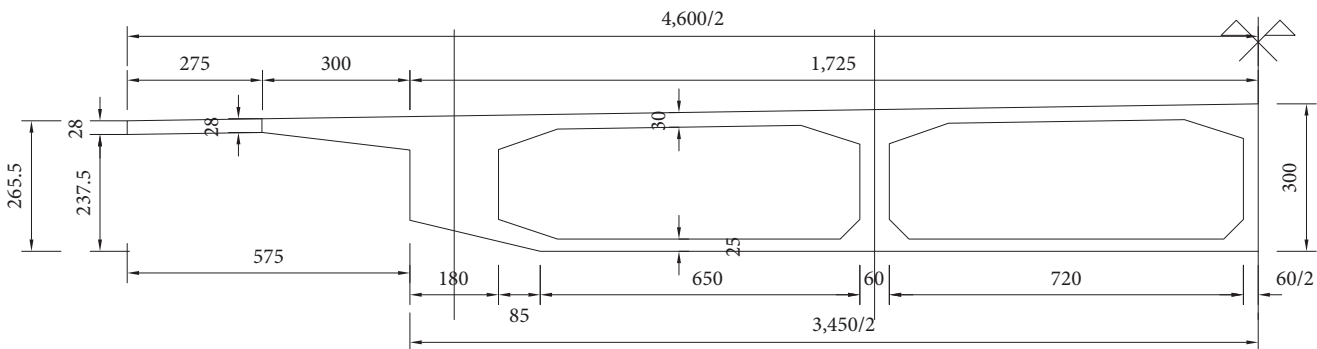


FIGURE 4: Standard cross-section of side span prestressed concrete box girder.

has a width of 46 m, and the nonstandard cross-section of the tower is 34.5 m in width. The main span and varied cross-section are shown in Figures 3 and 4.

2.3. Steel–Concrete Joint. Due to the differences in the materials of side span and main span and the stiffness discontinuity, stress tends to accumulate in the vicinity of steel–concrete joint of the hybrid girder. Besides, this section is found with a relatively large internal force, so it stands for a dangerous section and weak link of the entire bridge under structural stress [13–15], making it necessary to analyze force transfer mechanism in details. This bridge’s steel–concrete joint adopts C50 low shrinkage concrete-filled rear bearing structure. The joint

has a length of 2 m; a transitional steel girder is set between the steel girder and the steel–concrete joint; an inverted T-shaped rib stiffener is set up in the U ribs of top and bottom plates for transition. Meanwhile, the thickness of top and bottom plates is increased by 4 mm, while the web plate is thickened by 6 mm. When transferring the force, the steel girder distributes the force to the transitional steel girder through the thickened top and bottom plates and the inverted T-shaped rib stiffener, and the transitional steel girder then transfers the PBL (the term comes from the German word *Perfobond Leiste* and the English word is *Perfobond Strips ‘PBS’*) shear key composed by bearing plate, steel lattice, shear stud, and indoor concrete to the concrete filled and further to the concrete girder.

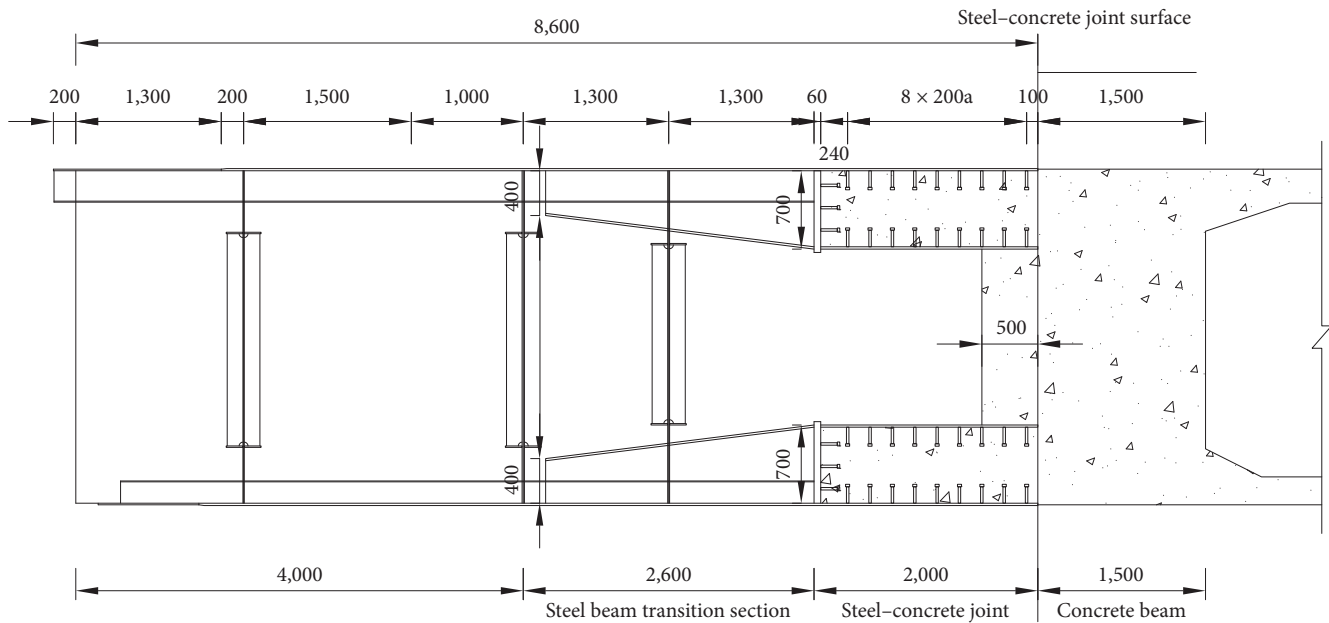


FIGURE 5: Elevation of steelconcrete joint.

By more firmly connecting steel lattice and the concrete filled with welding studs, prestressed steel strands are adopted for reinforced connection between the steelconcrete joint and the steel box girder. Considering the welding space, platforms required by the processing of various components, the area required by the concrete filled to disperse stress, and other factors, the height of steel lattice is reasonably determined as 700 mm. The inverted T-shaped reinforced rib has a length of 2.6 m, and its height transits from 0.4 to 0.7 m at the steelconcrete joint. When extending to the side span, the steelconcrete joint passes through the 1.5 m solid beam first, and then transits to the box girder via the chamfer, whose elevation is shown in Figure 5.

3. Overall Calculation under Different Loads and Calculation Results

3.1. Loading Conditions and Calculations. Moreover, MIDAS CIVIL is adopted for establishing the finite element model of the full-bridge truss. Specifically, beam elements are employed for the tower and main girder; the tensile-only truss element is utilized as the stayed cable. The steel–concrete joint is simulated by means of composite section, and the relative slipping between the steel plate and the concrete is not considered. The whole bridge consists of 1,152 nodes and 1,230 elements. The overall finite element model is shown in Figure 6.

In order to determine the loading force of the steel box girder at the cantilevered end, the steelconcrete joint is selected for extracting the dangerous cross-sections under six loading conditions, namely, the maximum bending moment (Load 1), the minimum bending moment (Load 2), the maximum axial force (Load 3), the minimum axial force (Load 4), the maximum torque (Load 5), and the minimum torque (Load 6). During the analyses, moving loads of automobiles and populations are converted into static loads through the moving load

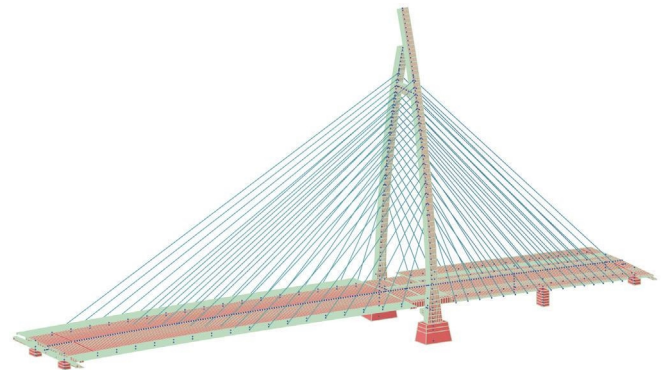


FIGURE 6: Finite element model of the whole bridge.

tracker, which are then applied to the model. These six static loads are combined with the constant load, respectively, to get the abovementioned six desired loads. The internal force results of the cross-section at the cantilevered end under six loading conditions are shown in Table 1.

It can be seen from Table 1 that the shearing force is relatively smaller than the axial force because the steelconcrete joint is located near the tower, and the horizontal components of the main and side spans are all transmitted to the joint, thus stabilizing the joint as a transition. It can also be known that the torque is also smaller than the bending moment, so the structure is mainly exposed to the bending effect at the cross-section of the steel box girder.

3.2. Overall Calculation Results of Midas Model. The envelopes of the bending moment and axial force of the main girder under the standard combinations are shown in Figures 7 and 8, respectively. It can be seen from these envelopes that at the steel–concrete joint, the structure is subject to large

TABLE 1: The internal force of the cantilever end section under different loading conditions.

Load	Axial force (kN)	Shearing force (kN)	Torque (kNm)	Bending moment (kNm)	Lateral bending moment (kNm)
Load 1	-4,290	19.7	-18.0	-8,460	-2,730
Load 2	-10,800	12.1	-27.7	-28,500	-1,740
Load 3	-4,310	19.8	-18.1	-8,770	-2,750
Load 4	-6,510	7.4	-10.4	-18,500	-1,040
Load 5	-4,360	-9.9	-745	-9,650	-1,230
Load 6	-7,020	-316	-9,200	-15,500	-13,300

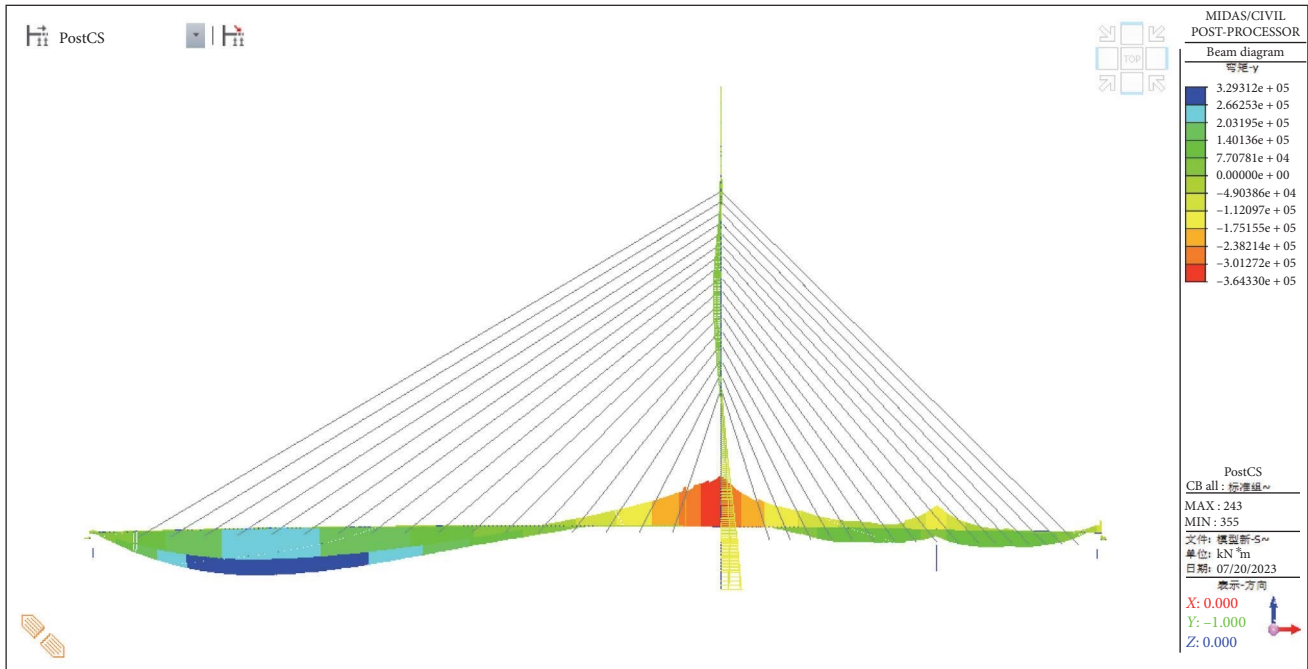


FIGURE 7: Envelope of bending moment of the main girder.

negative bending moment and axial force, and the axial force of the structure suddenly changes here due to the sudden changes in the stiffness. Therefore, it is necessary to establish a refined plate and shell solid model for stress analysis of the steel-concrete joint.

4. Refined Finite Element Model of Steel-Concrete Joint

As a kind of large general finite element software, ANSYS can be used for analyzing the solid elements of plate and shell, and is especially suitable for the detailed analysis of the steel-concrete joint. Therefore, ANSYS is adopted for the detailed analysis of the structure. According to the Saint Venant's Principle, the steel-concrete joint adopts six times of girder height (namely, with a length of 18 m) to avoid the impact of the stress concentration at the constraints on the analytical results [16, 17]. Likewise, 18 m steel-concrete joint is extracted along the side-span direction, and the entire model has a full length of 36 m.

4.1. Element Selection. The shell element shell181, the solid element solid185, and the link element link8 are, respectively, adopted for simulating the steel structure, the concrete, and

the prestressed reinforcement in the finite element model; the steel plate is mainly divided into rectangular grids, while the solid concrete is divided into hexahedral grids to ensure the calculation accuracy. The initial strain theory is employed for applying the prestress [18–20], and initial strain is set up for link8. In this paper, due to the complex model and large size, the entire structure is divided into 785 one-dimensional elements, 5,13,437 two-dimensional elements, and 1,191,776 three-dimensional solid elements. The finite element model is presented in Figure 9.

4.2. Material Properties. The material characteristic values for the concrete used are shown in Table 2, and the material characteristic values for the steel are shown in Table 3. The materials are all assumed to be linear and elastic in nature, and calculations are performed using the linear elastic constitutive model.

4.3. Boundary Conditions and Constraints. Since the chosen concrete girder passes through the fulcrum of the bridge tower, so the actual constraint applied on the model at the cross beam of the tower fulcrum, namely, U_x along the central axis of the bridge, U_y along the transverse direction, and

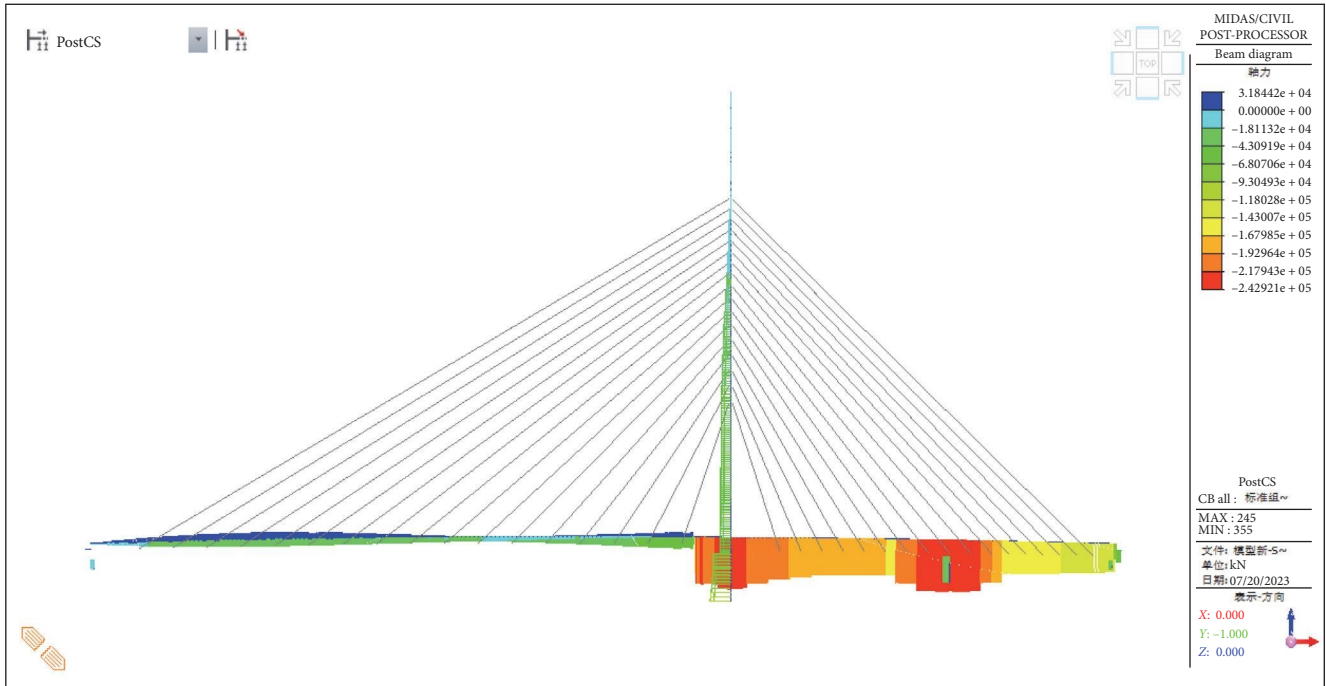


FIGURE 8: Envelope of axial force of the main girder.

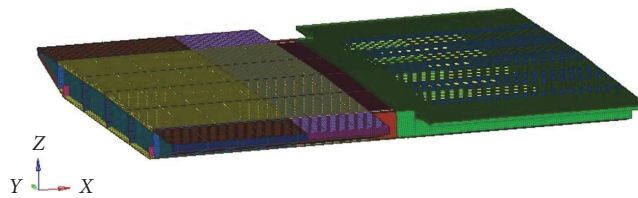


FIGURE 9: Finite element model of steel–concrete joint.

TABLE 2: Material characteristic values for concrete.

Structure	Material	Elastic modulus (GPa)	Poisson's ratio	Tensile strength (MPa)	Compressive strength (MPa)
Prestressed concrete box beam	C50 low-shrinkage concrete	34.5	0.2	2.65	32.4
Bridge deck pavement layer	UHPC	43.4	0.2	7	84

TABLE 3: Material characteristic values for steel.

Structure	Material	Elastic modulus (GPa)	Poisson's ratio	Tensile yield strength (MPa)	Compressive yield strength (MPa)
Steel box beam	Q345qD	34.5	0.3	345	345
Steel strand	Low-relaxation high-strength steel strand	40	0.3	1,860	410

U_z along the vertical direction, as is shown in Figure 10 by a red color. The concrete girder of the model is consolidated, and all nodes of the girder are constrained (constraints U_x , U_y , and U_z), as is shown in Figure 10 by blue color. No constraint is applied on the steel girder but it serves as the cantilevered end to apply the load. In order to apply the load on the steel-box girder conveniently, CERE command is utilized on all nodes of

the cantilevered end so that all nodes of the cross-section will function as the slave nodes, and the node at the core as the master node; the area between the slave nodes and the master node is defined as the rigid area, as is shown in Figure 10 by white color, and the element mass21 is established on the master node to apply the load. In order to apply the torque and bending moment on the element mass,

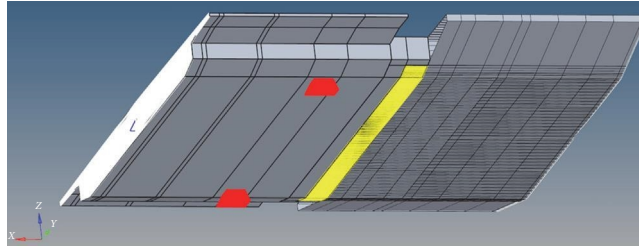


FIGURE 10: Constraint diagram of finite element model.

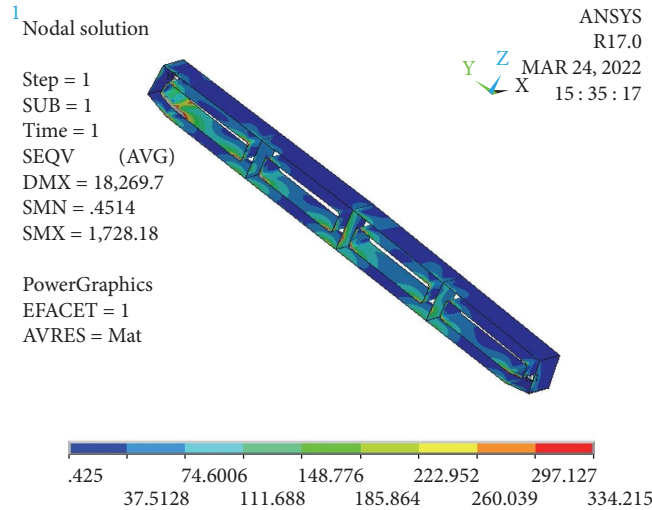


FIGURE 11: Von-mise stress of steel lattice.

TABLE 4: Stress of steel lattice under different load combinations.

Load	Maximum tensile stress along the bridge's central line (MPa)	Maximum compressive stress along the bridge's central line (MPa)	Maximum tensile stress perpendicular to the bridge's central line (MPa)	Maximum compressive stress perpendicular to the bridge's central line (MPa)	Von-mise stress (MPa)
Load 1	37.87	-107.37	45.58	-98.74	297.13
Load 2	36.67	-183.33	63.75	-181.50	293.38
Load 3	123.16	-307.90	78.89	-223.64	299.53
Load 4	143.16	-291.63	178.38	-115.88	306.71
Load 5	136.01	-312.35	174.22	-277.67	310.55
Load 6	120.34	-301.99	252.74	-281.67	324.05

keyopt(3) of mass21 is set as 0; that is, this element contains a total of six degrees of freedom, including translational degree of freedom and rotational degree of freedom. Constraint equations (presented by yellow color in Figure 10) are adopted for coupling of the adjacent nodes between the steel lattice and the concrete filled for the steelconcrete joint, but the sliding between them is not considered.

5. ANSYS Calculation Results of Steel–Concrete Joint

5.1. *Stress Results of Steel Plates in the Steel Lattice.* The von-mise stress nephogram of the steel lattice under the maximum bending moment is shown in Figure 11. The stress values

under other loads are listed in Table 4 (where the stress concentration on the joint surface is neglected, the same below).

It can be seen from Table 4 that the maximum von-mise stress of the steel lattice is 297.13 MPa. Specifically, the maximum tensile and compressive stresses along the central axis of the bridge are 37.87 and -107.34 MPa, respectively; the maximum tensile and compressive stresses along the transverse direction are 45.58 and -98.74 MPa, respectively, which do not reach the yield stress (345 MPa) of the steel plate, so the steel structure is basically under elastic force.

From Table 4, it can also be seen that under load cases 2–6, the maximum tensile stress of the steel lattice is 324.05 MPa, and the maximum compressive stress along the bridge's

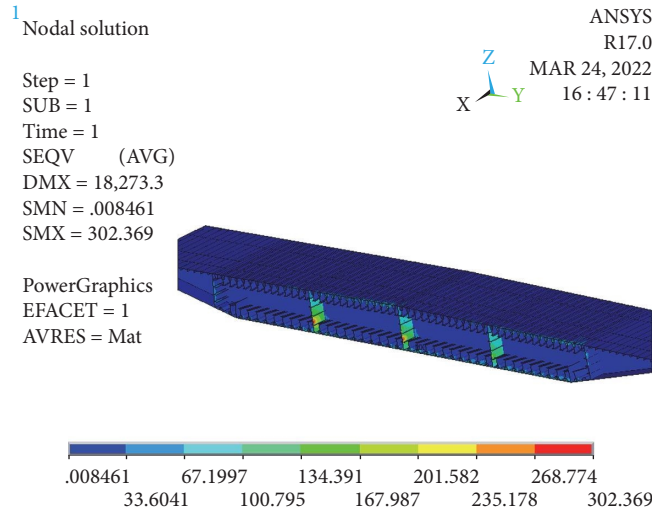


FIGURE 12: Von-mise stress of the steel part in the steel–concrete joint.

TABLE 5: Stress of the steel part in the steelconcrete joint under.

Load	Maximum tensile stress along the bridge’s central line (MPa)	Maximum compressive stress along the bridge’s central line (MPa)	Maximum tensile stress perpendicular to the bridge’s central line (MPa)	Maximum compressive stress perpendicular to the bridge’s central line (MPa)	Von-mise stress (MPa)
Load 1	125.39	−326.53	112.06	−132.49	302.37
Load 2	170.22	−301.44	148.83	−176.17	357.70
Load 3	126.09	−328.08	112.59	−133.12	303.83
Load 4	129.89	−309.99	116.97	−136.08	331.27
Load 5	247.20	−286.93	186.32	−176.02	315.48
Load 6	266.67	−281.96	287.75	−289.23	336.71

central line is 307.9 MPa, both of which do not exceed the yield strength of the steel and meet the specification requirements.

5.2. *Stress Results of Steel Plate in the Transitional Steel Girder.* The von-mise stress nephogram of the transitional steel girder under maximum bending moment is presented in Figure 12. The stress values under other loads are shown in Table 5.

It can be known from Table 4 that the maximum von-mise stress of the steel girder is 336.71 MPa. To be specific, the maximum tensile and compressive stresses along the central axis of the bridge are 266.67 and −326.53 MPa, respectively; the maximum tensile and compressive stresses along the transverse direction are 287.75 and −289.23 MPa, respectively. The maximum stress of the transitional steel girder is much larger than that of the steel lattice. Although the structure is still in the elastic stage, the maximum von-mise stress and the maximum compressive stress along the central axis of the bridge are close to the yield stress (345 MPa) of the steel plate.

5.3. *Stress Results of Concrete Filled in the Steel Lattice.* The principal tensile stress nephogram of the concrete filled under the maximum bending moment is shown in Figure 13. The stress values under other loads are shown in Table 6.

The behavior of prestressed steel reinforcement anchored on the pressure plate is simulated in this study using a coupling approach between one-dimensional truss elements and shell elements. However, this approach inevitably leads to stress concentrations in the vicinity of the prestressed anchor point on the pressure plate and the concrete. In practical engineering, the prestressed steel reinforcement is anchored on the pressure plate using anchorages, which allows for a more uniform transmission of prestress to the concrete through the pressure plate. Therefore, the stress concentration near this localized region should be excluded from the computed results. As shown in Figure 13, the maximum principal tensile stress in the filled concrete at the joint does not exceed 2.02 MPa over a larger area. To be specific, the maximum tensile stresses along the central axis and the transverse directions are 2.40 and 2.19 MPa, respectively, which do not exceed the designed standard tensile stress (2.65 MPa) of C50 concrete, suggesting that the concrete is basically in the elastic state. The maximum compressive stresses of the concrete filled in the joint along the central axis and the transverse directions are −2.26 and −16.62 MPa, respectively, with the maximum compressive stress of −17.54 MPa; compared to the mechanical properties of C50, the stress is lower, so the concrete is basically in the elastic state.

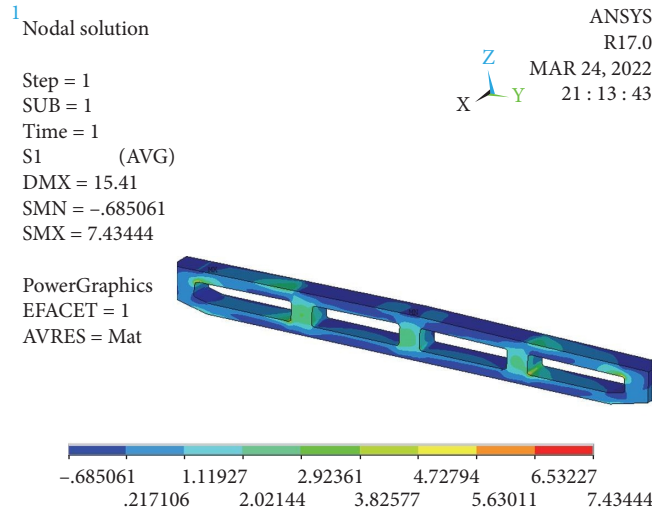


FIGURE 13: Principal tensile stress of concrete filled in the joint.

TABLE 6: Stress of concrete filled in the joint under different load combinations.

Load	Maximum tensile stress along the bridge's central line (MPa)	Maximum compressive stress along the bridge's central line (MPa)	Maximum tensile stress perpendicular to the bridge's central line (MPa)	Maximum compressive stress perpendicular to the bridge's central line (MPa)	Maximum principal stress (MPa)
Load 1	2.39	-2.12	2.05	-14.61	2.02/-15.30
Load 2	2.30	-2.26	2.62	-16.62	2.59/-17.54
Load 3	2.40	-2.12	2.06	-14.63	2.03/-15.32
Load 4	1.99	-2.18	2.10	-15.00	2.07/-15.72
Load 5	2.40	-2.13	2.07	-14.72	2.02/-15.42
Load 6	2.52	-2.20	2.19	-15.52	2.51/-16.40

Note: Maximum tensile stress is positive, while maximum compressive stress is negative.

6. Optimization of the High-Stress Area of Steel–Concrete Joint Structure

It can be seen from the calculation results that current calculated stresses of the steel plate and the concrete in the joint are relatively larger, especially for the steel plate, whose maximum von-mise stress exceeds 300 MPa. In order to significantly reduce the stress level of the steel plate in the joint and apply more reasonable load on the joint, by analyzing the sensitivity of the stress of the steel plate to the designed parameters, the thickness of the steel lattice web and the thickness of the bearing plate in the joint are chosen as the research variables. Under the condition of keeping other calculated parameters unchanged, the sensitivity of the steel plate stress to its thickness is analyzed. With 2 mm as the increase interval, the thickness of the web is increased from 24 to 40 mm; with 10 mm as the increase interval, the thickness of the bearing plate is increased from 60 to 100 mm.

6.1. *Thickness of the Web of the Steel–Concrete Joint.* When the thickness of the web is between 24 and 40 mm, the curves on how maximum stresses at different sites of the steel plate

change with the thickness of the web are presented in Figure 14, wherein S1 refers to the maximum stress of the top plate, S2 as the maximum stress of the bottom plate, S3 as the maximum stress of the web, and S4 as the maximum stress of the bearing plate, the same below.

It can be seen from the above figure that along with the increase in the thickness of the web in the joint, the stresses of the top and bottom plates basically remain unchanged, while the stresses of the web and bearing plate gradually decrease, and the stress of the web decreases faster. When the web thickness increases from 24 to 40 mm, the web stress reduces by 15.7%, and the bearing plate stress decreases by 8.15%, suggesting that the increase in the web thickness does not significantly reduces the high stresses of other sites.

6.2. *Thickness of the Bearing Plate of the Steel–Concrete Joint.*

The curves on how maximum stresses of different sites in the steel plate change with the bearing plate thickness are shown in Figure 15. It can be known that when the thickness of the bearing plate in the joint increases from 60 to 100 mm, the reduction in the stress of the top plate, bottom plate, web, and bearing plate reaches 44.9%, 33%, 26%, and 48.8%,

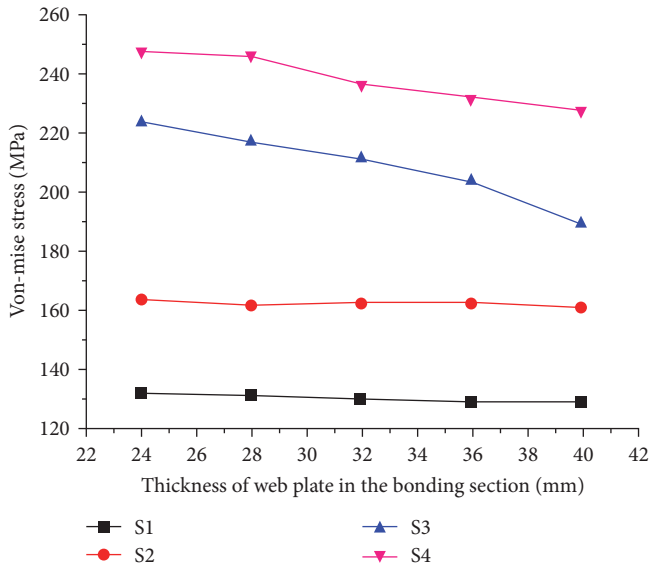


FIGURE 14: Variation of steel plate stress against thickness of mid web.

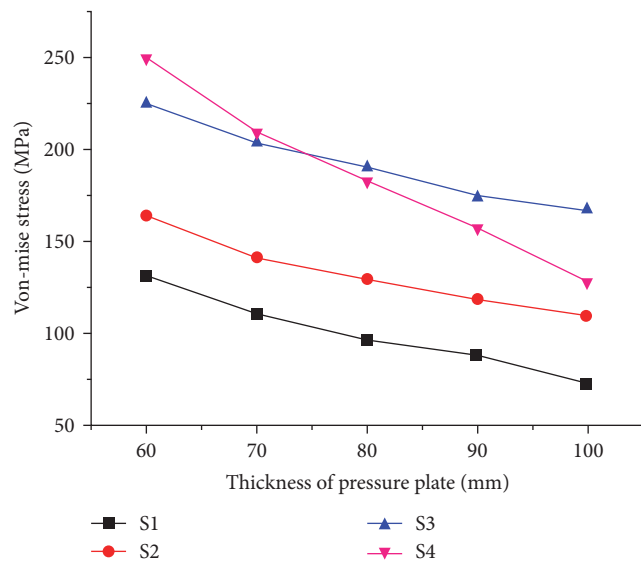


FIGURE 15: Variation of steel plate stress against thickness of bearing plate.

respectively. Therefore, by appropriately increasing the thickness of the bearing plate, it is ensured to greatly reduce the stress level of the steel plate in the joint without a great increase in the material costs.

6.3. Concrete Strength Grade of the Steel–Concrete Joint. When the concrete strength grade of the steel-mixed section is increased from C50 to C80, the stress change diagram of each part of the steel structure is shown in the Figure 16. It can be seen from the figure that when the concrete grade is increased from C50 to C60, the stress of the floor, web, and pressure plate decreases slightly, but the stress of the top plate increases slightly. When the concrete strength grade

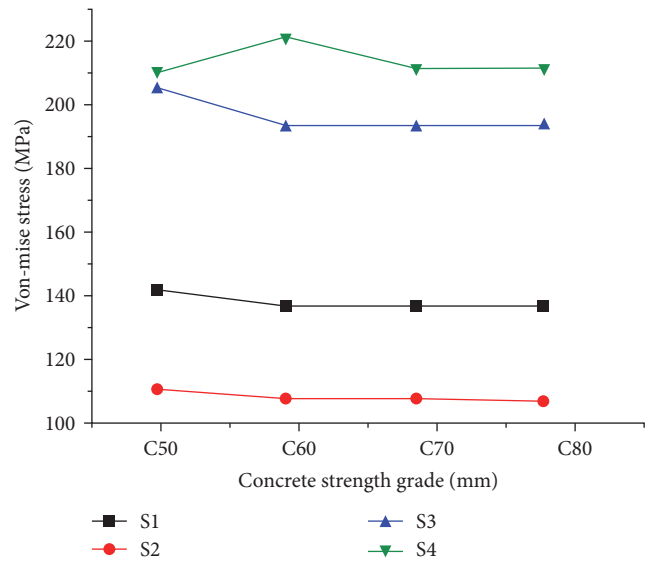


FIGURE 16: Variation of steel plate stress against thickness of bearing plate.

continues to increase, the stress of each part of the steel structure remains basically unchanged. Therefore, it can be inferred that for the steel mixed section structure of this bridge, the concrete strength grade is C50–C60, when the respective material characteristics of concrete and steel can be fully utilized.

7. Conclusions and Prospects

In this paper, a finite element method is adopted with midas for overall calculation and ANSYS for detailed analyses. Overall analysis is made on the single tower cable-stayed bridge, and the loading results of the steel–concrete joint of the main girder are imported into ANSYS to establish a refined model. The stresses of the steel–concrete joint under six unfavorable loading conditions are dissected, and reasonable suggestions on how to reduce the high stresses of the joint are offered based on the parameter sensitivity of the web and bearing plate’s thickness. Major conclusions are listed below:

- (1) The steel–concrete joint is adopted as the transitional part of the main girder for the single tower cable-stayed bridge. It is a reasonable scheme to achieve the smooth transition of the main span’s steel box girder and the side span’s concrete girder in terms of material and structural stiffness.
- (2) Based on the overall calculation results, the steel–concrete joint undertakes the task of transmitting the horizontal component of all stayed cables of the steel girder to the main girder of the prestressed concrete, while the concrete girder on the other end also transmits the great pressure to the joint through the prestressed reinforcement. The great pressure will combine the bearing plate, the steel lattice, and the concrete filled in a closer way, thus effectively reducing the relative

sliding between the steel and the concrete. Meanwhile, the concrete girder is subject to both the prestress and the horizontal stress of the stayed cable, giving better play to the strong stress tolerance of the concrete and making fuller use of all kinds of materials.

- (3) The refined finite element analysis results of the steel–concrete joint demonstrate that the stresses of the steel structure and the concrete are basically in the elastic state, but huge stress concentration is found at the connection of the steel lattice and the bearing plate, the corner of the top and bottom plates, the corner of the web, and the concrete filled. Therefore, local reinforcement shall be implemented during the design process, or the bevel smoothing shall be adopted for smooth corner transition and avoid stress concentration.
- (4) The sensitivity analysis of the joint web thickness and bearing plate thickness reveals that increasing the thickness of the intermediate web from 24 to 40 mm results in a significant 15.7% reduction in the stress of the web itself, while the stress in the steel member decreases by 8.15%. Conversely, increasing the thickness of the bearing plate from 60 to 80 mm leads to a notable reduction in stress for each part of the steel plate within the steel grid, with a maximum reduction of up to 48%.
- (5) When the concrete strength grade is elevated from C50 to C60, the stress in the bottom plate, web plate, and pressure plate decreases by 5%, while the stress in the top plate increases by 6%. As the concrete strength grade continues to increase, the stress in the steel structure components remains relatively stable. Consequently, the enhancement of concrete strength has a limited effect on reducing the stress in the steel grid, signifying that the design choice of C50 concrete strength grade for this bridge is rational and adequate.

Data Availability

The data used to support the findings of this study are available from the corresponding author upon request.

Conflicts of Interest

The authors declare that they have no conflicts of interest.

Acknowledgments

This research was supported by the Tianjin Transportation Commission and Tianjin Municipal Engineering Design & Research Institute (grant no. 2019B-26). The fourth author is grateful to the project of Tianjin Transportation Science and Technology Development Plan.

References

- [1] D. Lou, Y. Chen, Q. Feng, and J. Cai, “Analytical determination of static deflection shape of an asymmetric extradosed cable-stayed bridge using Ritz method,” *Materials*, vol. 15, no. 12, Article ID 4255, 2022.
- [2] Y. Zhang, Y. Li, H. Zhang et al., “Experimental study of distribution of stress and strain on pelvis in normal chinese adult,” *Sheng Wu Yi Xue Gong Cheng Xue Za Zhi*, vol. 14, no. 3, pp. 217–221, 1997.
- [3] V. Hoang, O. Kiyomiya, and T. An, “Experimental and numerical study of lateral cable rupture in cable-stayed bridges: case study,” *Journal of Bridge Engineering*, vol. 23, no. 6, Article ID 05018004, 2018.
- [4] A. Si Larbi, A. Gabor, and E. Ferrier, “Assessment of the long-term shear behavior of epoxy polymer lap joint used to bond steel and concrete composite structure,” *Journal of Composite Materials*, vol. 45, no. 4, pp. 459–477, 2011.
- [5] Y. Q. Liu, C. Chen, and S. J. Zheng, *Anchorage Structure of Composite Pylon*, China Communications Press, 2010.
- [6] Q. Zhu, Y. L. Xu, and K. M. Shum, “Stress-level buffeting analysis of a long-span cable-stayed bridge with a twin-box deck under distributed wind loads,” *Engineering Structures*, vol. 127, pp. 416–433, 2016.
- [7] Y. D. Yao, Y. Q. Yang, Z. B. Liu, Q. H. Pu, and Z. Shi, “Finite element analysis of steel and concrete joint section of railway hybrid box girder cable-stayed bridge,” *Qiao Liang Jian She, Qiao Liang Jian She*, vol. 45, no. 1, 2015.
- [8] X. Z. Li, L. Xiao, X. Zhang, and D.-J. Liu, “Experiment and research on bearing capacity of PBL shear connectors of steel–concrete composite joint,” *Ha’Erbin Gong Ye Da Xue Xue Bao*, vol. 4, pp. 181–186, 2009.
- [9] X.-Q. Yang and Y. Li, “Test study of bearing capacity of PBL shear connectors,” *Qiao Liang Jian She*, vol. 45, no. 1, 2015.
- [10] X. Tan, Z. Fang, and X. Xiong, “Experimental study on group effect of perfobond strip connectors encased in UHPC,” *Engineering Structures*, vol. 250, Article ID 113424, 2022.
- [11] Y.-L. Xu, *Wind Effects on Cable-Supported Bridges*, John Wiley & Sons, 2013.
- [12] J. He, Y. Liu, and B. Pei, “Experimental study of the steel–concrete connection in hybrid cable-stayed bridges,” *Journal of Performance of Constructed Facilities*, vol. 28, no. 3, pp. 559–570, 2014.
- [13] M. Adachi and M. Nishiyama, “Analytical study on prestressed concrete sub-frame assembled by post-tensioning considering bond-slip characteristic between prestressing steel and concrete,” *Nihon Kenchiku Gakkai Kōzōkei Ronbunshū*, vol. 532, pp. 161–167, 2000.
- [14] A. El-Zohairy, H. Salim, and A. Saucier, “Experimental study on fatigue performance of steel-concrete composite girders,” in *Fracture, Fatigue, Failure and Damage Evolution*, J. Carroll, S. Xia, A. Beese, R. Berke, and G. Pataky, Eds., vol. 6 of *Conference Proceedings of the Society for Experimental Mechanics Series*, pp. 77–83, Springer, Cham, 2019.
- [15] H. Lee, J. Min, S. Cho, and W. Chung, “Lateral loading performance of the joint between a precast concrete girder and a steel pier,” *Engineering Structures*, vol. 198, Article ID 109551, 2019.
- [16] Y. Huang, *Numerical Assessments of Cracks in Elastic-plastic Materials*, vol. 4 of *Lecture Notes in Applied and Computational Mechanics*, Springer, Berlin, Heidelberg, 2002.

- [17] J.-M. Drezet, M. Rappaz, G.-U. Grün, and M. Gremaud, "Determination of thermophysical properties and boundary conditions of direct chill-cast aluminum alloys using inverse methods," *Metallurgical and Materials Transactions A*, vol. 31, pp. 1627–1634, 2000.
- [18] H. Huang, Y. Xian, W. Zhang, M. Guo, K. Yang, and K. Xi, "Analysis of wind-induced vibration of a spoke-wise cable-membrane structure," *Journal of Marine Science and Engineering*, vol. 8, no. 8, Article ID 603, 2020.
- [19] X. Wang, X. Wang, Y. Dong, and C. Wang, "A novel construction technology for self-anchored suspension bridge considering safety and sustainability performance," *Sustainability*, vol. 12, no. 7, Article ID 2973, 2020.
- [20] M. A. Yimer and T. W. Aure, "Numerical investigation of reinforced concrete and steel fiber-reinforced concrete exterior beam-column joints under cyclic loading," *Iranian Journal of Science and Technology, Transactions of Civil Engineering*, vol. 46, pp. 2249–2273, 2022.